ELSEVIER

Contents lists available at ScienceDirect

Journal of Membrane Science

journal homepage: www.elsevier.com/locate/memsci





Wetting indicators, modes, and trade-offs in membrane distillation

Allyson L. McGaughey*, Amy E. Childress

Sonny Astani Department of Civil and Environmental Engineering, University of Southern California, 3620 S. Vermont Avenue, Los Angeles, CA, 90089, United States

ARTICLE INFO

Keywords:
Membrane distillation
Wetting
Wetting modes
Wetting resistance
Wetting resistance/vapor flux trade-off

ABSTRACT

In this study, we propose and demonstrate a simple solute mass balance to determine vapor flux and liquid flux in membrane distillation for several membrane materials under baseline and wetting conditions. We observe that distillate salinity can increase due to an experimental artefact, but that liquid flux can be used to conclusively diagnose wetting, quantify wetting rates, and indicate the relative number of wetted pores. We identify two wetting modes: "constant wetting", characterized by increasing distillate salinity and constant liquid flux, and "increasing wetting", characterized by increasing distillate salinity and increasing liquid flux. Constant wetting indicates that isolated pores remain wetted throughout operation, while increasing wetting indicates that more pores wet over time. Constant wetting may be tolerable at low liquid flux, requiring no intervention and resulting in or trade-off between wetting resistance and water production. In contrast, increasing wetting requires intervention. Reducing membrane pore size or increasing thickness can increase wetting resistance and delay liquid flux – but can also reduce vapor flux, resulting in trade-offs between wetting resistance and vapor flux. These results provide new understanding of wetting modes and trade-offs in membrane distillation and can guide membrane design and operation, for conventional and challenging applications.

1. Introduction

1.1. Background

Membrane distillation (MD) is a thermally driven membrane process that has shown promise for the treatment and reclamation of challenging feed streams, including those with high salinity (e.g. refs. [1–9]). Compared to reverse osmosis, the driving force in MD is only slightly reduced by feed stream salinity [9,10]. In MD, a warmer feed stream and a cooler distillate stream flow on opposite sides of a hydrophobic membrane. Under ideal conditions, the membrane pores are unwetted and support a vapor gap between the feed and distillate streams. The partial vapor pressure difference across the membrane drives water in the feed stream to evaporate, diffuse through the unwetted pores, and condense in the cooler distillate stream [6–8]. However, under real conditions, the membrane pores may become wetted; if this happens, the liquid feed stream can permeate through the membrane and freely mix with (contaminate) the distillate stream [7,11,12]. If pore wetting becomes significant, solute rejection may become less than ideal.

Characterization of wetting is key to elucidate the relationship between wetting resistance, membrane properties, solution chemistry, and operating conditions. Wetting resistance can be characterized using *ex*

situ or in situ characterization techniques. In ex situ characterization, membrane wetting resistance is determined based on measurements performed outside the MD process (e.g., membrane material characterization or liquid entry pressure (LEP) characterization). In in situ characterization, membrane wetting is determined during the MD process, enabling characterization of membrane wetting resistance while the membrane is subject to actual operating conditions. In situ characterization not only determines wetting resistance for the specific wetting mechanisms occurring in MD, but also enables real-time intervention.

1.2. Ex situ characterization of membrane wetting resistance

Membrane material characterization is often used to assess wetting resistance, and commonly, membrane hydrophobicity (characterized by contact angle measurement) is the indicator. Membrane hydrophobicity depends on the material, with polytetrafluoroethylene (PTFE) being the most hydrophobic polymer that is commonly used [13–15]; PVDF and PP membranes are less hydrophobic but also commonly used. Pore size is another key membrane property that has been used as an indicator of wetting resistance. Nominal pore sizes of MD membranes typically range between 0.2 and 0.45 μm [10].

LEP, or transmembrane pressure at which liquid enters a membrane

E-mail addresses: amcgaugh@usc.edu (A.L. McGaughey), amyec@usc.edu (A.E. Childress).

^{*} Corresponding author.

pore, depends on both contact angle and pore size to characterize wetting resistance. LEP can be determined by modeling or measurement. Theoretical LEP (LEP $_{th}$) is described by the classic Young-Laplace model for cylindrical pores [16]:

$$LEP_{th} = \frac{-4B\gamma_{tv}\cos\theta}{d_{p}} \tag{1}$$

where B is a pore geometry factor, γ_{lv} is liquid-vapor surface tension, θ is contact angle, and d_p is pore size. For PTFE membranes, which are characterized by an interconnected pore space with pore entrances formed by intersecting fibrils, LEP_{th} can be determined by the Kim-Harriott model [17]:

$$LEP_{th} = \frac{-4\gamma_{lv}}{d_p} \frac{\cos(\theta - \alpha)}{1 + \frac{d_F}{d_p}(1 - \cos\alpha)}$$
 (2)

where d_p is surface pore size, d_F is fibril diameter, and α is angle of the liquid meniscus entering the pore. LEP_{th} is typically reported as the minimum LEP, which corresponds to wetting of the largest membrane pore. Measured LEP (LEP_m) is also typically reported as the minimum LEP, or the lowest transmembrane pressure at which wetting is detected. Wetting has been detected by visual observation of liquid flow or droplets [10,17–19] and by measurement of solute passage [20,21].

Discrepancies between LEP values and wetting during MD have been observed; membranes with high LEP_m or LEP_{th} have still wetted during MD [22] and membranes with low LEPth have not wetted during MD [23]. For LEP_m, this may be in part because when wetting detection relies on visual observation, a very low initial flowrate [10] or small droplet [17,18] may not be easily visible and this may result in delayed wetting detection. Depending on how quickly transmembrane pressure increases, delayed wetting detection can result in overestimation of LEP_m. For this reason, measurement of solute passage may provide a more sensitive indicator for LEP_m. Also, because LEP experiments typically are not operated with the same feed stream conditions (e.g., temperature and salinity) that MD operates with, other discrepancies can occur. For example, lower temperatures in LEP measurement may increase surface tension and contact angles [24,25], resulting in overestimation of LEP_m [11]. Lower salinity generally decreases liquid-vapor surface tension [25,26]. However, solution chemistry in general can also affect liquid-solid interactions and contact angles [27], potentially resulting in conflicting effects of temperature and salinity on LEP. LEP may also depend on parameters that are not represented in the classic models. Guillen-Burrieza et al. [18] observed that LEP_m increases with membrane thickness; the authors suggest that increasing thickness may increase membrane mechanical strength, which may increase LEP_m. Yazgan-Birgi et al. [28] and Chamani et al. [19] developed LEP models based on computational fluid dynamics and genetic programming and predicted increasing LEPth with increasing membrane thickness. However, to the best of our knowledge, the effect of membrane thickness on wetting during MD has not been studied experimentally and independent of other membrane properties.

Furthermore, as noted by Jacob et al. [22], LEP does not consider wetting mechanisms. While LEP may predict pressure-driven wetting, LEP may not predict surface-tension-, scaling-, or fouling-driven wetting because while transmembrane pressure is fairly constant along the membrane surface, concentration polarization and especially scaling/fouling may not be. Scaling/fouling may form or deposit on any area of the membrane surface – not necessarily at the largest pore – and initiate wetting. In our previous paper (i.e., McGaughey et al. [29]), we introduced an LEP distribution to incorporate pore size heterogeneity into wetting resistance for the first time. LEP distributions are particularly relevant when multiple pores become wetted before wetting is detected, and when wetting initiates at pores other than the single, largest pore. Still, LEP characterization has limitations for accurate prediction of wetting during MD and *in situ* characterization may better

describe wetting for different wetting mechanisms.

1.3. In situ characterization of membrane wetting

In early MD studies, some researchers used nonlinear trends in water production (i.e., changes in the net flux, or the combined flux of vapor, liquid, and dissolved solutes) as an indicator of wetting during MD [22, 30]. However, depending on transmembrane pressure, liquid flux may occur from the feed to the distillate side or vice versa. In MD, the transmembrane pressure may be positive or negative, depending on system configuration and operating conditions, especially if there are different flowrates on the feed and distillate sides. As noted by Christie et al. [31], while equivalent flow rates are often used for convenience, optimal energy efficiency and performance can be obtained by balancing heat capacity flow rates rather than volumetric flow rates. For positive transmembrane pressure, liquid flux is expected to increase net flux; for negative transmembrane pressure, liquid flux is expected to oppose vapor flux and decrease net flux (but may still result in solute passage via mixing of the feed and distillate streams). At zero transmembrane pressure, the thermal gradient is expected to drive liquid flux from the feed to the distillate side due to thermo-diffusion [32].

Wetting may also affect net flux indirectly. Partial wetting (i.e., partial liquid penetration into a pore that results in a thinner vapor gap between the feed and distillate streams [7,29,33]) may increase temperature and concentration polarization and reduce the driving force for vapor flux. Conversely, a thinner vapor gap may shorten the diffusion path length for water vapor, which may increase vapor flux [12,33–37]. Interestingly, increased vapor flux can also result from higher evaporation rates during partial wetting because the liquid-vapor interfacial area within interconnected pores is greater than it is at isolated pore entrances [33,36,37].

Operating with lower hydrophobicity and accepting partial wetting to achieve higher vapor flux is an example of the wetting resistance/ vapor flux trade-off in MD. Wetting resistance/vapor flux trade-offs in MD have recently been introduced and analyzed by Wang et al. [37], McGaughey et al. [29], and Li et al. [33]. Wang et al. [37] and Li et al. [33] showed that reduced membrane hydrophobicity results in reduced wetting resistance, but also can result in partial wetting, which increases vapor flux as discussed above. We (i.e., McGaughey et al. [29]) also showed a wetting resistance/vapor flux trade-off in that smaller pore sizes result in greater wetting resistance, but also lower permeability and vapor flux. For solution chemistries that are likely to form scale, reducing pore size can be more effective than increasing contact angle to achieve wetting resistance [29] - therefore, reducing pore size to increase wetting resistance to scaling-induced wetting is likely worth the trade-off of reduced vapor flux. Also, in past studies of MD with high-salinity feed streams, operating conditions have been adjusted to maintain lower vapor flux and reduce the potential for concentration polarization and scaling on the membrane surface, thereby preventing wetting [5,12]. Operating at lower vapor flux to prevent wetting also represents a wetting resistance/vapor flux trade-off in MD [29]. To the best of our knowledge, these are the only trade-offs between wetting resistance and vapor flux that have been discussed in the MD literature.

Due to the complexities in characterizing wetting by detecting changes in net flux, increasing distillate conductivity is often used as a wetting indicator during MD [22,38]. Guillen-Burrieza et al. [39] and Couto et al. [40] reported the slope of distillate conductivity over time as a wetting rate. However, distillate conductivity measurements and wetting rates based on conductivity do not have meaningful units and provide limited quantitative understanding of solute passage. Guillen-Burrieza et al. [39] also mention the use of a mass balance to convert the shope of the distillate conductivity into a "leak rate"; however, results are not shown.

Solute rejection, calculated from conductivity measurements, is perhaps the most common indicator of membrane wetting, although not always discussed in the context of wetting. MD is generally considered to

provide complete rejection of non-volatile solutes. However, because ideal (100%) rejection is not typically measured, researchers have used various arbitrary definitions of rejection (e.g., rejection >99% [11,41,42], >99.9% [11,43–45], or >99.98% [46]) to indicate membranes are performing adequately. Similarly, sudden changes in rejection (e.g., ref [47]) as well as arbitrary rejection minimums (e.g., 99.5% [48,49] or 97% [50]) have been used to define wetting.

Alternative in situ detection methods and wetting indicators have also been explored. In 2017, Chen et al. [51] developed a method for wetting detection based on electrochemical impedance spectroscopy. As liquid penetrates one or more pores, the vapor gap thins, and transmembrane impedance is reduced. Thus, the onset of partial wetting can be indicated by a reduction in transmembrane impedance [51]. When full wetting occurs, for one or more pores, transmembrane impedance is zero. However, due to the asymptotic nature of the impedance curve as it approaches zero, the transition to full wetting may be difficult to distinguish. And because impedance does not depend on salinity or the number of wetted pores, neither quantitative wetting rates nor solute flux can be obtained from impedance curves. Also in 2017, Ahmed et al. [52] detected wetting based on electrical current measurement using a conductive membrane [11,52]. Similar to impedance spectroscopy, current measurements indicate the onset of wetting but do not describe wetting rates; also, this measurement can only be used for conductive membranes, which are not common for MD. In 2020, Jacob et al. [38] developed a method to detect wetting based on light transmission, enabling visualization of wetting locations and wetting propagation. The authors note that this method may be affected by operating parameters and has limited application to solution chemistries with scaling/fouling potential or those containing opaque particles. Membrane materials may also affect applicability.

Liquid flux, if it can be separated from net and vapor flux, may provide a wetting indicator with the benefits of simple detection (detection based on flux and conductivity measurements), as well as meaningful quantification of wetting rates in units of liquid mass per membrane area per time (as opposed to conductivity, impedance, or current), indication of the number of wetted pores via direct comparison to vapor flux, and facile quantification of solute flux for any feed stream solute. However, to the best of our knowledge, liquid flux versus time has not been previously reported in the MD literature – nor has vapor flux been distinguished from net flux.

1.4. Objectives

In this study, we propose and demonstrate a simple mass balance approach to characterize vapor and liquid flux in MD under baseline conditions (i.e., moderate salinity, without surface-tension-lowering constituents) and wetting conditions (i.e., with surface-tension-lowering constituents or high salinity). We present liquid flux as a wetting indicator and use it to define different types – or modes – of wetting in MD. Using these new wetting indicators and modes, we aim to identify membrane wetting (differentiated from experimental artefacts), identify tolerable and intolerable wetting under baseline and wetting conditions, quantify wetting rates, and compare vapor flux and liquid flux to indicate the relative number of wetted pores. Finally, we aim to bring to light trade-offs between wetting resistance and vapor flux that are due to pore size and membrane thickness – membrane properties that, compared to contact angle, have been less frequently studied with respect to wetting resistance.

2. Materials and methods

2.1. Membranes

Three commercial flat-sheet, microporous PTFE membranes (Parker Performance Materials, Lee's Summit, MO, USA) were used: QM050, a symmetric, single-layer membrane with a nominal pore size of $0.05 \mu m$;

QL822, a laminate membrane (PTFE selective layer and PP support layer) with a nominal pore size of 0.45 μm ; and QM022, a symmetric, single-layer membrane with a nominal pore size of 0.2 μm . Two commercial flat-sheet, microporous PP membranes (Sterlitech, Kent, WA, USA) with nominal pore sizes of 0.1 and 0.45 μm were used; both membranes were single-layer and symmetric. Also, three single-layer, electrospun membranes were used. All three electrospun membranes were fabricated from a 10 wt% blended polymer solution of PVDF and PVDF-co-hexafluoropropylene (PVDF-co-HFP) at a 6:1 ratio, dissolved in a 60:40 dimethylformamide:acetone mixture. The membranes were spun in the same apparatus and under identical conditions (i.e., with a tip-to-collector distance of 16 cm, flow rate of 2.2 mL/h, and voltage of 15 kV); different spinning durations were used to achieve different thicknesses with otherwise similar membrane properties.

2.2. Membrane characterization

A micrometer with an accuracy of $\pm 1~\mu m$ (MDC-1 PX, Mitutoyo, Kawasaki, Japan) was used to measure membrane thickness; ten measurements were made at arbitrary locations on three separate samples of each membrane. Bulk porosity was characterized via the gravimetric method as in Rao et al. [4]; porosity (ε) is given by:

$$\varepsilon = 1 - \frac{m_m}{\rho_n a_m \delta_m} \tag{3}$$

where m_m (g), a_m (m²), and δ_m (m) are the mass, surface area, and thickness of the membrane and ρ_p (g/m³) is polymer density [4]. Three separate samples of each membrane material were used to determine average bulk porosity. 2-D surface morphology was characterized for three arbitrary areas of the membrane surface using a field-emission scanning electron microscope (Nova NanoSEM 450, FEI, Hillsboro, OR, USA); ImageJ software (version 1.52, National Institutes of Health, Bethesda, MD, USA) was used to analyze the scanning electron microscopy (SEM) images to determine surface pore parameters. SEM images and surface pore size distributions for all membranes are shown in the Supporting Information (Figs. S1 through S6). Contact angle (θ) was measured according to the sessile drop method (with 5-µL drop volume) using a goniometer (Model 260, ramé-hart, Succasunna, NJ, USA); reported values represent an average of at least ten measurements. LEPth was determined using the Kim-Harriot LEP model (equation (2), with d_D equal to the maximum surface pore size) for the PTFE membranes and using the Young-Laplace model (equation (1), with dp equal to the maximum surface pore size) for the PP membranes. For the electrospun membranes, because thickness is not included in classic LEP models, LEP was characterized by LEP_m (described below).

$2.3. \ \ \textit{LEP measurement and MD performance characterization}$

A bench-scale MD system (Fig. 1) was used for LEP measurement and to characterize performance for all membranes and solution chemistries. In this study, we term the product water the "distillate/permeate stream", to account for both condensed water vapor (i.e., distillate) and liquid feed solution (i.e., permeate) that passes through the membrane via wetted pores. Membrane coupons were installed in a custom-built membrane module with an active area of 20 cm² and mesh spacers (Sterlitech, Kent, WA, USA) were placed in the feed and distillate/permeate channels to promote mixing and provide mechanical support. Deionized water was used as the distillate/permeate solution. Feed and distillate/permeate flowrates were held constant at 0.76 L/min in countercurrent configuration. Feed and distillate/permeate temperatures were kept constant using a recirculating heater and chiller. Data were recorded every 30 s using a custom data acquisition and control program created in LabView (National Instruments, Austin, TX, USA).

LEP experiments were conducted at a constant operating temperature of 25 \pm 1 $^{\circ}C$ on both the feed and distillate/permeate sides.

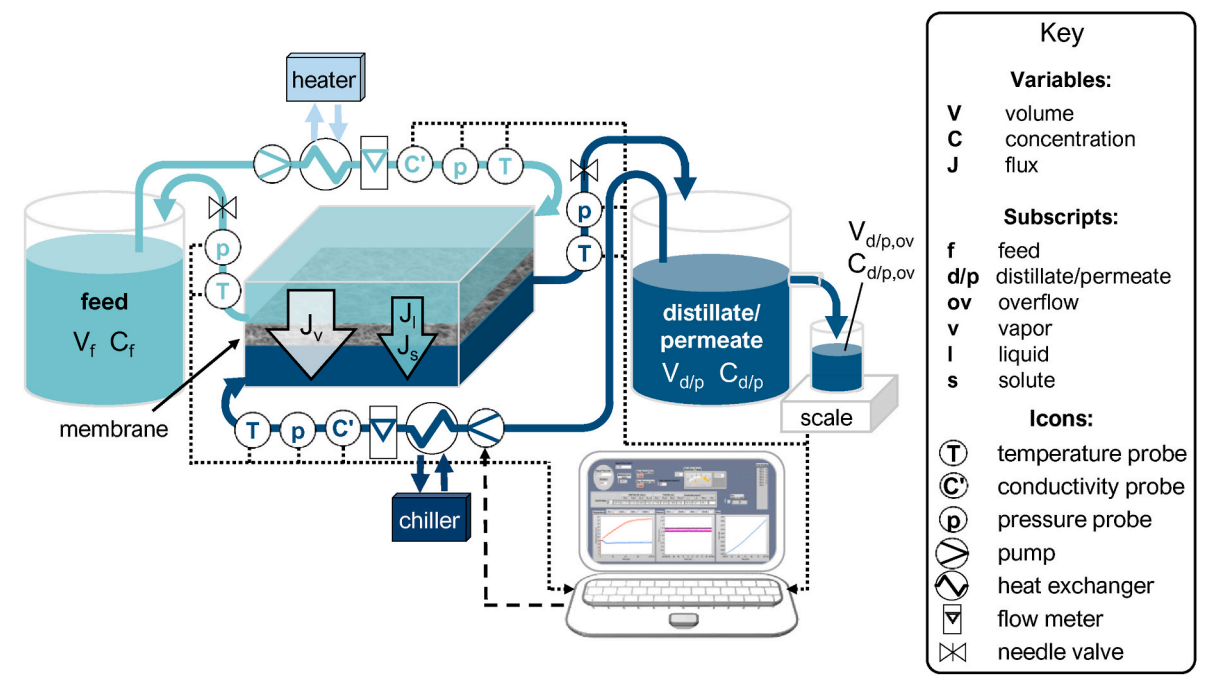


Fig. 1. Diagram of bench-scale MD system indicating system configuration and key variables.

Transmembrane pressure (ΔP) was calculated as the feed-stream pressure (i.e., the average of measured pressures at the inlet and outlet of the module on the feed side) minus the distillate/permeate-stream pressure (i.e., the average of measured pressures at the inlet and outlet of the module on the distillate/permeate side). To increase ΔP , the feed-stream pressure was increased using a needle valve (McMaster-Carr, Elmhurst, IL, USA). The measured LEP was defined as the highest ΔP recorded prior to or when a sudden increase in the distillate/permeate concentration occurred.

For performance characterization experiments, temperatures and pressures were allowed to stabilize over a 1-h startup period. Averaging over the duration of all experiments, operating temperatures were $52\pm2~^\circ\text{C}$ on the feed side and $17\pm1~^\circ\text{C}$ on the distillate/permeate side. Pressures were controlled using needle values to maintain near-zero transmembrane pressure; gauge pressures were 12 ± 1 and 12 ± 2 kPa on the feed and distillate/permeate sides. For baseline experiments, 1 M NaCl was used as the feed solution and the feed stream was periodically diluted with deionized water to maintain constant concentration. For all other experiments, the feed stream was not diluted in order to assess the effect of increasing solute concentration on wetting. For surfactant-driven wetting experiments, 200-ppm Triton X-100 (Sigma-Aldrich, St. Louis, MO, USA) in 1 M NaCl was used as the feed solution. For scaling-driven wetting experiments, 5-M NaCl was used as the feed solution.

The bulk feed solute concentration (C_f) and the bulk distillate/permeate solute concentration ($C_{d/p}$) were calculated from measured conductivities using standard curves prepared with NaCl solutions of known concentrations. Seven concentrations with conductivities between the minimum (0 μ S/cm) and maximum (200 μ S/cm) of the measurement range of the distillate/permeate conductivity probe and seven additional concentrations with conductivities between the minimum (0 mS/cm) and maximum (200 mS/cm) of the measurement range

of the feed conductivity probe were selected. For both probes, three samples of each concentration were prepared and used to generate three standard curves, which were averaged; all standard curve R^2 values were at or above 0.997. We note that dissolved CO_2 is also known to impact conductivity; effects can be significant at low salinities and elevated pressures. Börner et al. [53] showed that the effect is negligible at 0 MPa applied pressure for salinities of 0.001–0.98 M NaCl. In the current study, applied pressures were 0.01 MPa and the effect of dissolved CO_2 on conductivity was assumed to be negligible.

Concentration polarization was estimated according to refs. [54,55]:

$$C_{f,m} = C_f \exp\left(\frac{J_w}{\rho_f K}\right) \tag{4}$$

where $C_{f,m}$ (mol/L) is the feed solute concentration at the membrane surface, J_W (kg/m²s) is water flux, ρ_f (kg/m³) is the density of the feed solution, and K (m/s) is the film mass-transfer coefficient. K was determined from the Sherwood correlation developed by Gustafson et al. [541:

$$K = 0.023 \frac{Re^{0.8} Sc^{1/3} D}{d_H} \tag{5}$$

where Re (dimensionless) is the Reynolds number, Sc (dimensionless) is the Schmidt number, D (m 2 /s) is the solute diffusion coefficient, and d_H (m) is the hydraulic diameter of the flow channel. d_H was calculated based on the effective channel height to account for the presence of spacers according to the method developed and validated by Gustafson et al. [54] for a similar membrane, module, and MD system.

In all experiments, the volume of the distillate/permeate stream in the system $(V_{d/p})$ was held constant at 2.14 L; this volume was selected such that the initial liquid level in the distillate/permeate tank was immediately below the overflow line. Therefore, as vapor and/or liquid

pass through the membrane from the feed stream to the distillate/permeate stream, an equivalent quantity of liquid overflows the distillate/permeate tank through the overflow line. Overflow was collected in the overflow collection vessel on a scale (shown in Fig. 1) and mass was recorded every 30 s. Net flux (J_{net} in kg/m²h) is given by:

$$J_{net} = \Delta m_{d/p,ov} / a_m \Delta t \tag{6}$$

where $\Delta m_{d/p,ov}$ (kg) is mass of distillate/permeate stream collected in the overflow collection vessel over time interval Δt (h), with $\Delta t = t_{i+1} - t_i$ held constant at 30 s. a_m (m²) is membrane area.

Solute flux (J_s in kg/m²h) is determined according to:

$$J_{s} = \frac{V_{d/p} \Delta C_{d/p} + C_{d/p,ov,t_{i+1}} V_{d/p,ov,t_{i+1}} - C_{d/p,ov,t_{i}} V_{d/p,ov,t_{i}}}{a_{m} \Delta t}$$
(7)

where $V_{d/p}$ (m³) is volume of distillate/permeate stream in the system, $\Delta C_{d/p}$ (kg/m³) is change in concentration of the distillate/permeate stream in the system over time interval Δt , and $C_{d/p,ov,t_i}$ and $V_{d/p,ov,t_i}$ are concentration and volume of the distillate/permeate stream overflow at time t_i . As noted previously, $V_{d/p}$ is held constant over time. Also, it is assumed that liquid flux occurs from the feed to the distillate/permeate side because in the absence of significant transmembrane pressure, the thermal gradient is assumed to drive mass transfer via thermo-diffusion [32].

Solute concentration in the overflow collection vessel at time t is calculated by:

$$C_{d/p,ov,t} = \frac{\sum_{i=1}^{i=t} C_{d/p,i} V_{d/p,i}}{V_{d/p,ov,t}}$$
(8)

assuming that the solute concentration of the distillate/permeate stream overflowing during the time step Δt is the same as the solute concentration of the distillate/permeate stream in the system at time t (i.e., assuming that the distillate/permeate stream is fully mixed).

Liquid flux (J_l in kg/m²h) is calculated by:

$$J_l = \rho_f \left(\frac{J_S}{C_{f,m}} \right) \tag{9}$$

assuming that ρ_f is approximately constant, that the permeate concentration is equal to $C_{f,m}$, and that $C_{f,m}$ is approximately constant during time step Δt so $C_{f,m}$ is taken as the average $C_{f,m}$ over the time step Δt .

Vapor flux $(J_v \text{ in kg/m}^2\text{h})$ is calculated by:

$$J_{v} = J_{net} - J_{l} \tag{10}$$

Unless indicated otherwise, net, liquid, and vapor flux are calculated every 30 s and are shown as moving averages with a period of 10 min. Rejection (*R*, unitless) is calculated according to refs. [56,57]:

$$R = 1 - \frac{\left(C_{d/p,t_{i+1}} V_{d/p,tot,t_{i+1}} - C_{d/p,t_i} V_{d/p,tot,t_i}\right)}{\left(C_{f,t_{i+1}} V_{d/p,tot,t_{i+1}} - C_{f,t_i} V_{d/p,tot,t_i}\right)}$$
(11)

where C_{f,t_i} indicates the concentration of the feed stream at time t_i and $V_{d/p,tot,t_i}$ indicates the total volume of the distillate/permeate stream at

Table 1Material characterization results for the three commercial PTFE membranes. ± values (when given) represent standard deviation.

Membrane	QM050	QL822	QM022
θ (°) ^a	144 ± 5	144 ± 4	142 ± 7
Thickness (µm)	61 ± 7	180 ± 6	68 ± 7
Bulk porosity (%)	84 ± 0.5	70-85 ^b	87 ± 0.2
Maximum surface pore size (µm)	1.0 ± 0.1	2.4 ± 0.04	1.2 ± 0.1
Minimum LEP _{th} (kPa) ^a	137	65	112

^a Contact angles and minimum LEP values are shown for pure water at 25 °C.

time t_i . For all parameters, percent differences were calculated as $\frac{x-y}{(x+y)/2}$.

3. Results and discussion

3.1. Commercial PTFE membranes

3.1.1. PTFE membrane characterization

Table 1 shows material characterization results for the three commercial PTFE membranes. All three membranes have similar measured contact angles and bulk porosities. The unsupported QM050 and QM022 membranes also have similar thicknesses. The supported QL822 membrane has greater total thickness, but smaller selective layer thickness (approximately $34\pm2~\mu m$, as measured after carefully peeling the selective layer from the support layer). The maximum surface pore size is smallest for the QM050 membrane, intermediate for the QM022 membrane, and largest for the QL822 membrane. Given that the membranes have similar contact angles, based on maximum surface pore sizes, minimum LEPth values are lowest for the QL822 membrane, intermediate for the QM022 membrane, and highest for the QM050 membrane.

3.1.2. PTFE membrane baseline performance characterization

The data in Fig. 2 show the performance of the three PTFE membranes under baseline conditions (i.e., with 1 M NaCl feed solution) for one day of operation. Graphs in the first row (Figs. 2a, b, and c) show $C_{d/p}$ over time. Fewer data points are shown for the QM022 membrane compared to the QM050 and QL822 membranes because a smaller overall change in $C_{d/p}$ was observed for the QM022 membrane, and the minimum detectable concentration change for the distillate/permeate conductivity probe is limited to approximately 0.05 mg/L.

For all three membranes, $C_{d/p}$ increases during operation. However, the mode of increase is different for each membrane. For the QM050 membrane (Fig. 2a), $C_{d/p}$ increases initially and then levels off at a constant concentration after 11 h of operation. For the QL822 membrane (Fig. 2b), $C_{d/p}$ increases relatively linearly over time. For the QM022 membrane (Fig. 2c), $C_{d/p}$ increases gradually throughout operation, with slightly lower slope after 14 h. In the MD literature, increasing $C_{d/p}$ is typically considered a key indicator of membrane wetting. If experiments were run for a shorter duration (e.g., 5–10 h) as is often reported in the literature (e.g. refs. [42–44,47,58,59]), all three membranes would be considered to be wetted.

To quantify how much liquid water is passing through the wetted membrane pores, a solute mass balance is used to separate net flux (i.e., flux of vapor, liquid, and dissolved solutes) into vapor flux and liquid flux. Figs. 2d, e, and f show net flux and vapor flux versus time. For each membrane, net flux and vapor flux results are nearly identical and overlap (at this scale). Despite their different pore sizes (Table 1), net flux values for the QM050 and QM022 membranes are similar (24 $\pm\,2$ and 24 ± 1 L/m²h, averaged over the duration of each experiment). This is likely because the membranes have similar bulk porosity (Table 1). For smaller pore sizes and porosity, membrane permeability and net flux are expected to be lower [6]; however, researchers have observed that net flux is more sensitive to porosity than pore size [10]. Net flux for the QL822 membrane (21 \pm 1 L/m²h) is slightly lower than it is for the QM050 and QM022 membranes, likely due to the greater thickness of the QL822 membrane (Table 1), because permeability and net flux are generally lower for greater membrane thickness [6]. For all three membranes, net flux is relatively constant and stable with only a slight decrease over time. This is expected for moderate-salinity feed solutions without added foulants; the slight decrease in net flux may be due to trace amounts of foulants present in the deionized water used for the

The data in Figs. 2g, h, and i show liquid flux versus time. Given that the scale for liquid flux is approximately two orders of magnitude less than the scale for vapor flux and net flux (Figs. 2d, e, and f), it can be seen that the contribution of liquid flux to net flux is very low. This is

^b Bulk porosity for the QL822 membrane is manufacturer-reported.

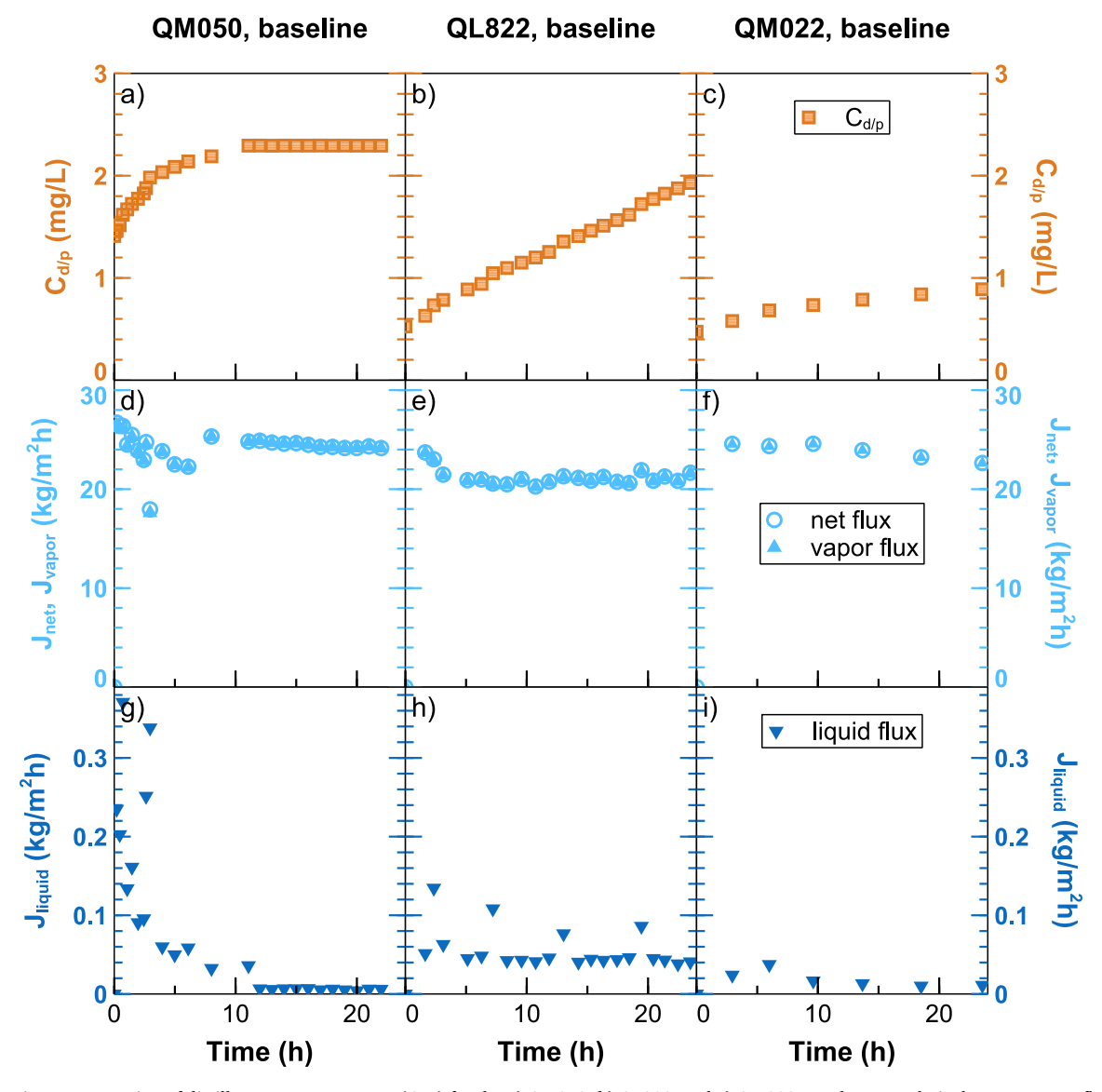


Fig. 2. Increasing concentration of distillate/permeate stream ($C_{d/p}$) for the **a**) QM050, **b**) QL822, and **c**) QM022 membranes; relatively constant net flux and vapor flux for the **d**) QM050, **e**) QL822, and **f**) QM022 membranes; and different trends in liquid flux versus time for the **g**) QM050, **h**) QL822, and **i**) QM022 membranes. All membranes were operated under baseline conditions (i.e., with 1 M NaCl feed solution). For each row, legends are shown in the right-hand graph (i.e., graphs c, f, and i).

likely why liquid flux has been overlooked and it has been convention to refer only to vapor that passes through the membrane – because permeate mass may be considered negligible compared to distillate mass. However, quantification of liquid flux, even when values are very small, is important for wetting characterization, and especially for early identification of wetting.

For the QM050 membrane (Fig. 2g), liquid flux fluctuates initially, then decreases until 12 h of operation; after 12 h of operation, liquid flux is approximately 0 kg/m²h. If it is assumed that all increases in $C_{d/p}$ and liquid flux (Figs. 2a and g) are due to wetting, these results would

suggest that the membrane was initially wetted (liquid flux occurred) and then became unwetted (liquid flux stopped). However, spontaneous reversal of wetting is not known to occur in MD; pore wetting is generally understood to be irreversible without intervention (e.g., drying and replacing membranes, backwashing with air [12,60]). Therefore, it appears that the initial increase in $C_{d/p}$ in Fig. 2a is due to factors other than pore wetting. Although small increases in $C_{d/p}$ are not often discussed in the MD literature, especially compared to larger changes in $C_{d/p}$ (or in rejection) observed in wetting studies, small initial decreases in rejection have been noted (e.g., Rajwade et al. [49]). We suggest that

the initial increase in $C_{d/p}$ observed here (Fig. 2a) represents a common, vet so far unidentified, experimental artefact. In the current study, before the beginning of each experiment, the system is drained and the distillate/permeate loop is rinsed via pumping with deionized water until conductivity remains below 2 µS/cm for several hours. Then, the system is drained again, and new deionized water is added to the distillate/permeate tank. As experiments progress, the deionized water added at the beginning of the experiment may slowly mix, via pumping, with any liquid remaining in the distillate/permeate loop (e.g., within heat exchangers or fittings), resulting in $\mathcal{C}_{d/p}$ that initially increases and then levels off over time. As $C_{d/p}$ approaches a constant value, liquid flux appears to decrease. Thus, the decreasing liquid flux in Fig. 2g indicates that increasing $C_{d/p}$ is likely due to this experimental artefact, which we term "solute mixing". It is only with observation of liquid flux data that fluctuations in $C_{d/p}$ occurring as a result of operating techniques (representing experimental artefacts), can be conclusively distinguished from solute passage due to wetting (representing membrane performance).

For the QL822 membrane (Fig. 2h), liquid flux is relatively constant throughout operation. Constant liquid flux along with the increasing linear trend in $C_{d/p}$ (Fig. 2b) indicate that increases in $C_{d/p}$ are not due to solute mixing but that full wetting of one or more pores has occurred. Also, constant liquid flux (Fig. 2h) indicates that the wetting mode is stable (at least over the duration shown). Therefore, we refer to this increasing $C_{d/p}$ and constant liquid flux as "constant wetting" mode. Notably, the much greater magnitude of vapor flux (Fig. 2e) compared to liquid flux (Fig. 2h) indicates that the majority of pores are unwetted and only permit vapor flux. As the QL822 membrane has similar contact angle but larger maximum surface pore size compared to the nonwetting QM050 membrane (Table 1), and because wetting occurs at moderate salinity and in the absence of surface-tension-reducing constituents, wetting is attributed to spontaneous wetting of one or more larger, isolated pores. These larger pores likely have lower LEP that permits liquid entry under baseline conditions – i.e., there is insufficient wetting resistance due to the membrane properties.

For the QM022 membrane (Fig. 2i), liquid flux increases initially, then decreases from 6 to 18.5 h of operation, and finally remains relatively constant from 18.5 to 24 h of operation. Although liquid flux for the QM022 membrane is low from 18.5 to 24 h of operation (average of $0.01~\text{kg/m}^2\text{h}$, Fig. 2i), it is approximately double the liquid flux for the QM050 membrane over the same time period (average of $0.005~\text{kg/m}^2\text{h}$, Fig. 2g). The decrease in liquid flux from 6 to 18.5 h of operation, followed by constant liquid flux (Fig. 2i) may indicate a combined effect of solute mixing and wetting. Solute mixing may appear as initially increasing liquid flux that subsides; then, wetting of some membrane pores results in constant liquid flux at a lower rate. Again, the much greater magnitude of vapor flux (Fig. 2f) compared to liquid flux (Fig. 2i) indicates that the majority of pores are unwetted and only permit vapor flux.

3.1.2.1. Alternative in situ wetting indicators. The data in Figs. 3a, b, and c show NaCl rejection over time. For all membranes, excepting statistical outliers, NaCl rejection is always greater than 99%. As discussed previously, researchers have used various arbitrary quantitative definitions of rejection (e.g., rejection >99% [11,41,42], >99.9% [11,43–45], or >99.98% [46]) to indicate membranes are performing adequately, or arbitrary rejection minimums (e.g., 99.5% [48,49] or 97% [50]) to define wetting. Notably, the trends that are clearly visible in liquid flux data (Figs. 2g, h, and i) are not apparent in rejection data (Figs. 3a, b, and c). Thus, rejection is a less sensitive wetting metric than liquid flux

and may have less utility for early detection of wetting or wetting in short-term experiments.

Unlike rejection, results for the rate of change of distillate/permeate conductivity (i.e., $\Delta C'_{d/p}/\Delta t$, Figs. 3d, e, and f) clearly follow the same trend as liquid flux (Figs. 2g, h, and i). Thus, the rate of change of $C'_{d/p}$ can serve as a proxy for liquid flux, especially if the solute mass balance cannot be solved to obtain liquid flux (e.g., if the initial volume of the distillate/permeate solution and/or the relationship between conductivity and concentration are unknown). However, the rate of change of $C'_{d/p}$ does not have meaningful units. Thus, we see that liquid flux is a preferable wetting metric to enable quantitative understanding of wetting rates, direct comparison to vapor flux, and facile calculation of solute flux.

3.1.3. PTFE membrane wetting characterization

The data in Fig. 4 show the performance of the QM022 membrane exposed to a surfactant-containing feed solution and the QM022 and QM050 membranes exposed to a high-salinity (5 M NaCl) feed solution. In all three experiments, $C_{d/p}$ increases exponentially over time (Figs. 4a, b, and c). The increase is different – both in magnitude and in trend – from $C_{d/p}$ versus time for these membranes under baseline conditions (Figs. 2a and c). The variability in both net and vapor flux (Figs. 4d, e, and f) is likely due to gradual wetting of membrane pores at different rates, and, for the high-salinity feed solution, scaling on the membrane surface that can cause pore blockage and wetting. Also, in all three experiments, liquid flux increases over time (Figs. 4g, h, and i) and is greater than it is under baseline conditions (Figs. 2g, h, and i), but is still much lower than vapor flux (Figs. 4d, e, and f), which indicates that the majority of pores remained unwetted.

The exponential increases in $C_{d/p}$ (Figs. 4a, b, and c) and liquid flux (Figs. 4g, h, and i) indicate that more pores become wetted over time, resulting in increasing liquid and solute flux; we refer to this as "increasing wetting". Increasing wetting mode occurs for both surfactant- and scaling-induced wetting. For the surfactant-containing feed solution, wetting is attributed to reduced surface tension of the solution that results in an LEP lower than the transmembrane pressure for some pores. As the bulk and surface concentrations of surfactant in the feed solution increase over time due to vapor flux, surface tension and LEP continue to decrease: the result is wetting of an increasing number of pores. Increasing wetting trends have been previously observed for feed solutions with reduced surface tension; Lin et al. [59] noted that wetting became progressively worse as surfactant concentration increased and Wang et al. [48] observed exponentially decreasing rejection for alcohol- and surfactant-driven wetting. For the high-salinity (scaling) feed solution, wetting is attributed to salt crystallization on the membrane surface [7,11,12]. After scaling occurs, salt crystals reduce the effective contact angle of the membrane surface. As additional crystals nucleate and grow, scaling may cause wetting of additional pores. Also, as suggested by Gryta [61,62], scaling-induced wetting of large pores may initiate wetting of smaller pores adjacent to deposits, resulting in "progressive wetting" [61,62].

For scaling-induced wetting, even though the QM050 membrane has smaller pore size (Table 1) and greater wetting resistance under baseline conditions (Fig. 2) compared to the QM022 membrane, both membranes wet in increasing wetting mode. However, the onset of liquid flux for the QM050 membrane (Fig. 4i) is delayed compared to the QM022 membrane (Fig. 4h), likely also due to its smaller pore size (Table 1). Interestingly, smaller pore size does not result in lower vapor flux for the QM050 membrane compared to the QM022 membrane, through 4 h

¹ Results for the QM022 membrane exposed to surfactant-containing and high-salinity feed solutions are single experiments that were previously performed in triplicate; the average data for distillate conductivity and net flux from the triplicate experiments were shown in our previous publication (i.e., McGaughey et al. [29]) for comparison of the performance of the QM022 membrane to coated membranes.

operation (Figs. 4e and f). As mentioned previously, this is likely because both membranes have similar bulk porosity (Table 1). These results build on the wetting resistance/permeability trade-off due to pore size introduced in our previous paper (i.e., McGaughey et al. [29], by quantifying the trade-off (based on vapor and liquid flux) for membranes with similar hydrophobicity, thickness, and bulk porosity but different pore sizes. The results also demonstrate that the trade-off may be possible to overcome for membranes with different pore sizes, but similar bulk porosity.

3.2. Commercial PP membranes

3.2.1. PP membrane characterization

To investigate the wetting modes for different membrane materials, and to further investigate the role of pore size, two commercial PP membranes (designated PP1 and PP2) were used. Characterization results for the PP membranes are shown in Table 2. Contact angle, thickness, and bulk porosity values are relatively similar for both membranes. The PP2 membrane has a larger maximum surface pore size and lower minimum LEP value compared to the PP1 membrane. Both membranes have relatively low minimum LEP values.

3.2.2. PP membrane baseline performance characterization

The data in Fig. 5 show the performance of both PP membranes under baseline conditions (i.e., with 1 M NaCl feed solution). For both membranes, $C_{d/p}$ and liquid flux (Figs. 5a and c) increase exponentially throughout operation, indicating increasing wetting mode. Because

wetting occurs at baseline conditions, in the absence of surface-tension-lowering constituents and scaling, wetting is attributed to insufficient wetting resistance and increasing wetting is likely due to gradual wetting of smaller pores that are adjacent or connected to larger pores that wet under baseline conditions, as suggested by Gryta [61,62] for scaling-induced wetting. The slower increase in $C_{d/p}$ and liquid flux for the PP1 membrane compared to the PP2 membrane is likely due to its smaller pore size.

Because increasing wetting mode is observed under baseline conditions (unlike the PTFE membranes, for which increasing wetting mode was only observed for solution-chemistry-driven wetting) and because increasing wetting mode occurs for both PP membranes regardless of pore size, wetting mode is likely due to a material property of the PP membranes. If the PP membranes have greater pore interconnectivity (i. e., permeability in the direction parallel to the membrane surface [63]) compared to the PTFE membranes, then spreading of wetting liquid to adjacent pores would be expected. No matter the reason, the increasing wetting makes these PP membranes unsuitable for use in MD; however, they are useful for investigating the role of pore size in wetting resistance/vapor flux trade-offs.

The greater vapor and liquid flux for the PP2 membrane compared to the PP1 membrane (Figs. 5b and c), demonstrates the wetting resistance/permeability trade-off due to pore size, which was observed in our previous publication (i.e., McGaughey et al. [29]). In this study, we demonstrate the trade-off for membranes with different pore sizes but similar contact angles, thicknesses, and bulk porosities. At 8 h of operation, liquid flux is much lower for the PP1 membrane than it is for the PP2 membrane

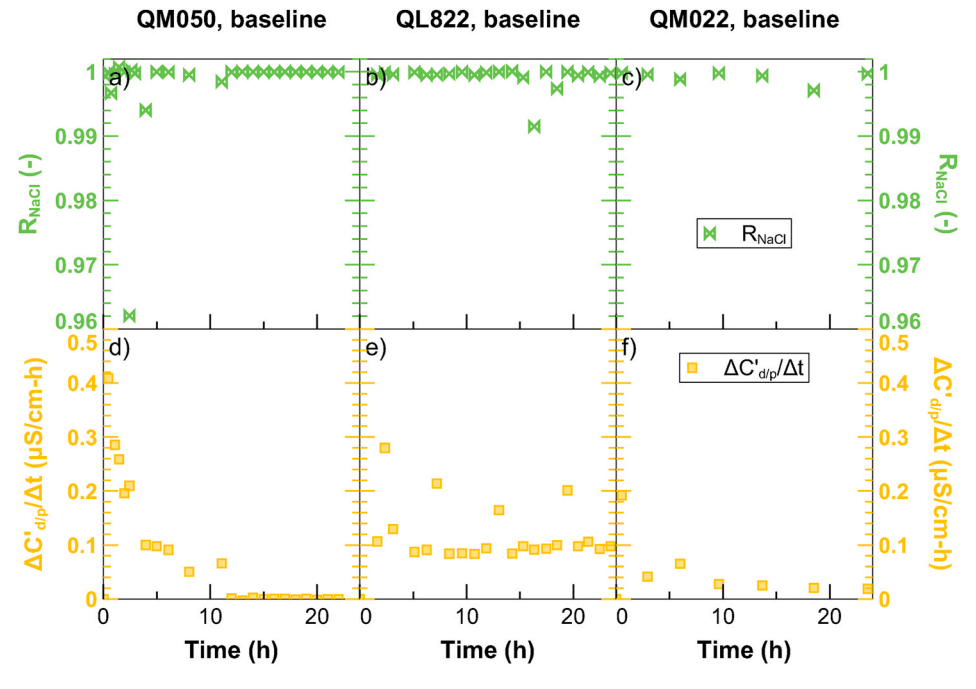


Fig. 3. Relatively constant NaCl rejection for the a) QM050, b) QL822, and c) QM022 membranes; different trends in the rate of change of distillate/permeate conductivity versus time (i.e., $\Delta C'_{d/p}/\Delta t$) for the d) QM050, e) QL822, and f) QM022 membranes. All membranes were operated under baseline conditions (i.e., with 1 M NaCl feed solution). For each row, legends are shown in the right-hand graph (i.e., graphs c and f).

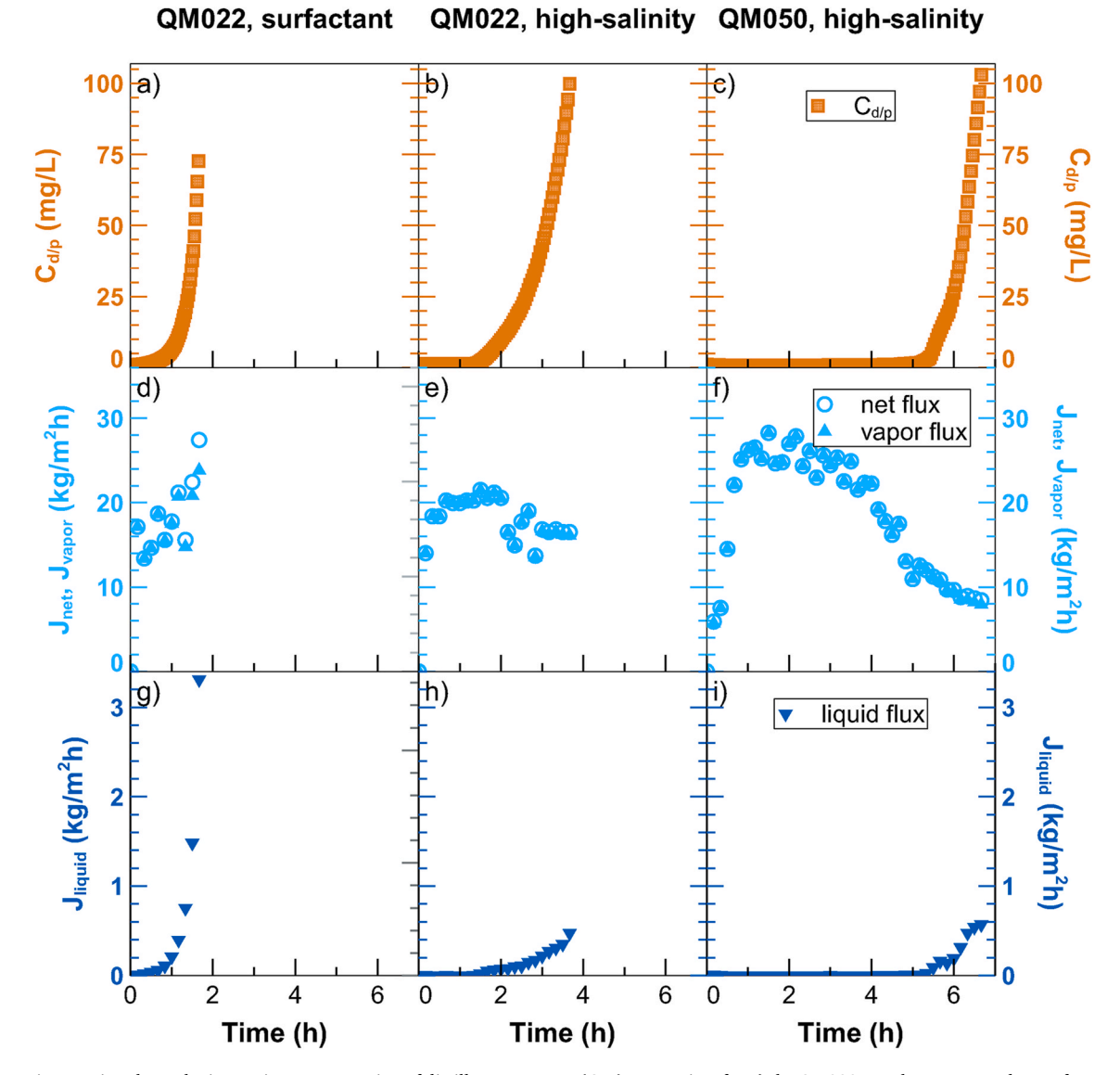


Fig. 4. Increasing wetting shown by increasing concentration of distillate/permeate ($C_{d/p}$) versus time for **a**) the QM022 membrane exposed to surfactant, and the **b**) QM022 and **c**) QM050 membranes exposed to high-salinity feed solution; relatively variable net flux and vapor flux for **d**) the QM022 membrane exposed to surfactant, and the **e**) QM022 and **f**) QM050 membranes exposed to high-salinity feed solution; and increasing liquid flux for **g**) the QM022 membrane exposed to surfactant, and the **h**) QM022 and **i**) QM050 membranes exposed to high-salinity feed solution. For each row, legends are shown in the right-hand graph (i.e., graphs c, f, and i).

(Fig. 5c); the percent difference is approximately 200%. At the same time, the percent difference in vapor flux (Fig. 5b) for the PP1 membrane compared to the PP2 membrane is only 67%. Thus, pore size has a greater effect on liquid flux than on vapor flux. This is likely due to differences between the dependence of mass transfer resistance on pore size for vapor diffusion versus liquid flow through membrane pores.

3.3. Electrospun membranes

3.3.1. Electrospun membrane characterization

To investigate a third membrane material, as well as to assess the role

Table 2 Material characterization results for the commercial PP membranes. \pm values (when given) represent standard deviation.

PP1	PP2
126 ± 2	124 ± 3
107 ± 3	107 ± 4
75 ± 3	81 ± 1
1.4 ± 0.2	2.4 ± 0.5
9	6
	126 ± 2 107 ± 3 75 ± 3 1.4 ± 0.2

^a Contact angles and minimum LEP values are shown for pure water at 25 °C.

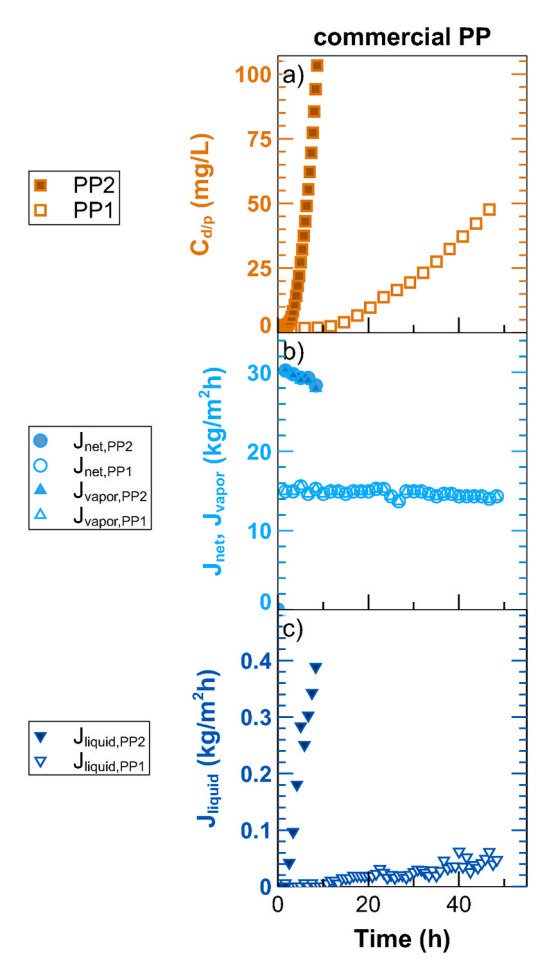


Fig. 5. a) Increasing wetting shown by increasing concentration of distillate/permeate stream $(C_{d/p})$ versus time, **b)** relatively constant net flux and vapor flux, and **c)** increasing liquid flux for the commercial PP membranes at baseline conditions (i.e., with 1 M NaCl feed solution).

Table 3 Material characterization results for the three electrospun membranes. \pm values (when given) represent standard deviation.

Membrane	ES1	ES2	ES3
θ (°)	138 ± 2	139 ± 2	138 ± 4
Thickness (mm) Surface porosity (%) Maximum surface pore size (µm) LEP _m (kPa)**	$\begin{array}{c} 0.29 \pm 0.03 \\ 34 \pm 7 \\ 2.3 \pm 0.6 \\ 57 \end{array}$	$\begin{array}{c} 0.60 \pm 0.03 \\ 41 \pm 3 \\ 2.6 \pm 0.3 \\ 88 \end{array}$	$\begin{array}{c} 0.81 \pm 0.10 \\ 38 \pm 2 \\ 2.4 \pm 0.3 \\ 80 \end{array}$

^{*}Contact angles are shown for pure water at 25 °C.

of membrane thickness in wetting mode, three electrospun membranes (designated ES1, ES2, and ES3) were used. As mentioned in section 2.1, the membranes were spun in the same apparatus and under identical conditions but with different spinning durations to achieve different thicknesses with otherwise similar membrane properties. Material characterization results (Table 3) show that the three membranes have similar contact angles, surface porosities, and maximum surface pore sizes, but different thicknesses and measured LEPs.

Because thickness is not included in classic LEP models (e.g., the Young-Laplace and Kim-Harriott models [17,18,28]), LEP was measured for each electrospun membrane (Table 3). Interestingly, measured LEP is

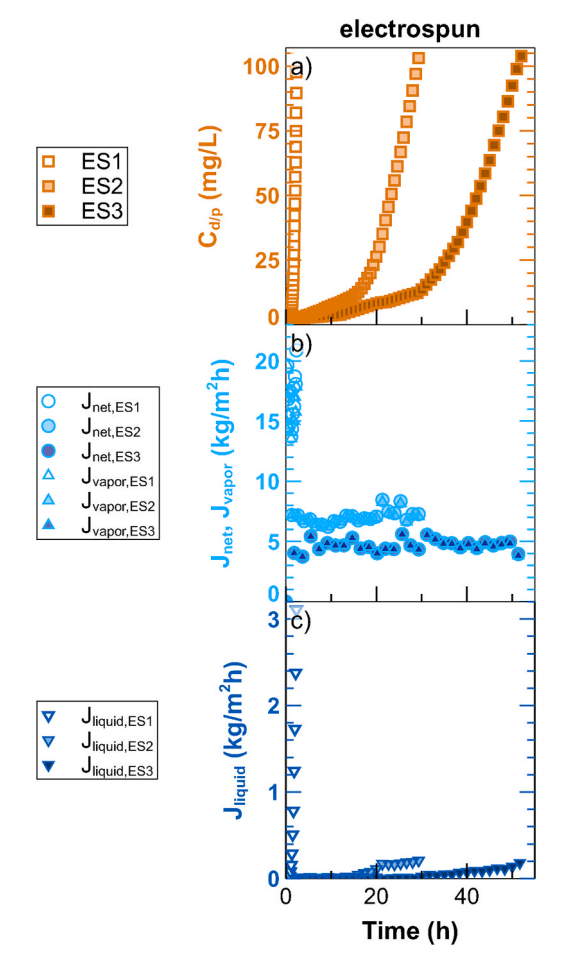


Fig. 6. a) Increasing wetting shown by increasing concentration of distillate/permeate stream $(C_{d/p})$ versus time; **b)** relatively constant net flux and vapor flux; and **c)** increasing liquid flux for the electrospun membranes at baseline conditions (i.e., with 1 M NaCl feed solution).

greater for the ES2 compared to the ES1 membrane, but not for the ES3 compared to the ES2 membrane. These results may support the LEP model developed by Chamani et al. [19], which predicts that initially, LEP increases linearly with membrane thickness but then LEP tapers off at greater thicknesses [19]. Chamani et al. [19] also find that greater membrane thickness results in lower liquid flux. Lower liquid flux may delay wetting detection and affect measured LEP, depending on the rate of increase of transmembrane pressure (as discussed in section 1.2). For all three electropsun membranes, transmembrane pressure was increased by less than 0.5 kPa/s; for the minimum detectable concentration change (0.05 mg/L), at a relatively low liquid flux of 0.01 kg/m²h, 20 s would be required to detect solute passage. Therefore, delayed wetting detection could result in differences of $\pm 10~\mathrm{kPa}$ in measured LEP values.

3.3.2. Electrospun membrane baseline performance characterization

The data in Fig. 6 show performance results for the three electrospun membranes under baseline conditions. $C_{d/p}$ and liquid flux increase exponentially for all membranes, indicating increasing wetting mode. Electrospun membranes are known to have a highly interconnected pore structure [64]; similar to the PP membranes, increasing wetting likely occurs due to progressive wetting of adjacent pores in the interconnected pore structure. Wetting of the electrospun membranes at baseline conditions is likely due to the relatively large maximum surface pore sizes of the electrospun membranes (Table 3), which are similar to

^{**}Measured LEP values are shown for 1 M NaCl solution at 25 °C.

the QL822 PTFE membrane (Table 1) that also wetted under baseline conditions (Fig. 2b). However, the electrospun membranes have much higher liquid flux compared to the QL822 membrane and eventually wet in increasing wetting mode, rendering them unsuitable for use in MD. Still, these membranes are useful for investigating the role of thickness in wetting resistance/vapor flux trade-offs.

The rate of change of $C_{d/p}$ and liquid flux is slower for the thicker membranes (Figs. 6a and c). Both vapor and liquid flux decrease with increasing membrane thickness for all three membranes (Figs. 6b and c) - likely because thicker membranes have reduced permeability to vapor and liquid. At 2 h of operation, liquid flux is much lower for the ES2 and ES3 membranes compared to the ES1 membrane; the percent difference is approximately 200% in both cases (Fig. 6c). At the same time, the percent differences in vapor flux are only 92 and 121% for the ES2 and ES3 membranes compared to the ES1 membrane (Fig. 6b). At 20 h of operation, the percent difference in liquid flux is 146% for the ES3 membrane compared to the ES2 membrane, but the percent difference in vapor flux is only 26%. Similar to pore size, thickness has a greater effect on liquid flux than on vapor flux. Again, this is likely due to differences between the dependence of mass transfer resistance on membrane thickness for vapor diffusion versus liquid flow through membrane pores. These results exemplify another wetting resistance/vapor flux trade-off in MD.

4. Conclusions and implications

In this study, we investigate detection and diagnosis of wetting in MD. While *in situ* wetting detection has long relied on measurement of distillate salinity, we observe that distillate salinity can increase due to an experimental artefact ("solute mixing"). Because solute mixing can obscure the onset of wetting, alternative methods for wetting detection are required. We propose and demonstrate a simple solute mass balance approach to characterize vapor flux and liquid flux in MD. As a wetting indicator, liquid flux enables diagnosis of wetting, quantification of wetting rates, and facile determination of solute flux. Direct comparison of liquid flux and vapor flux can indicate the relative number of wetted pores.

We define two modes of wetting in MD: "constant wetting", characterized by increasing $\mathcal{C}_{d/p}$ and constant liquid flux, and "increasing wetting", characterized by increasing $C_{d/p}$ and increasing liquid flux. Constant wetting mode indicates that a stable number of pores remain wetted throughout operation, while increasing wetting mode indicates that more pores wet over time. Notably, constant wetting may be tolerable without intervention. For recirculating systems, the product water will eventually reach a constant, terminal concentration $C_{d/p,\infty}$ (i. e., the concentration of the mixed distillate and permeate). For example, for the QL822 membrane, assuming constant net flux and liquid flux, $C_{d/p,\infty}$ is ~3.5 mg/L NaCl. If $C_{d/p,\infty}$ is acceptable, constant wetting is tolerable and does not require intervention. When wetting is tolerable, a wetting resistance trade-off does not exist: greater liquid flux will simply result in slightly greater net flux. In contrast, increasing wetting is expected to eventually result in wetting of all membrane pores with $C_{d/p}$ eventually equaling the feed stream concentration. Thus, increasing wetting requires intervention.

Increasing wetting mode is observed to occur regardless of differences in membrane pore size and thickness - although a delay in wetting is observed for smaller pore sizes and greater thicknesses. Vapor flux and liquid flux both generally decrease with decreasing membrane pore size and increasing membrane thickness; however, smaller pore sizes and increased membrane thickness have a greater effect on liquid flux than on vapor flux. These effects result in wetting resistance/vapor flux tradeoffs: increased wetting resistance due to smaller pore size or greater membrane thickness also results in reduced vapor flux.

These results have implications for membrane design and system operation for conventional and challenging applications. Depending on

whether water quality or water production is more important for a given application, reducing liquid flux may be desirable even at the cost of reduced vapor flux. Reducing pore size and/or increasing membrane thickness to achieve wetting resistance may reduce reliance on novel, higher-cost membrane materials and/or fabrication methods. For conventional applications, selection of a membrane material that maintains constant wetting mode is key to achieve reliable long-term performance. For challenging applications, modification of operating conditions or pretreatment may be necessary to prevent increasing wetting.

CRediT authorship contribution statement

Allyson L. McGaughey: Conceptualization, Investigation, Visualization, Writing – original draft, Writing – review & editing. Amy E. Childress: Conceptualization, Writing – review & editing, Supervision, Funding acquisition.

Declaration of competing interest

The authors declare that they have no known competing financial interests or personal relationships that could have appeared to influence the work reported in this paper.

Acknowledgements

Funding: this work was supported by the National Science Foundation [grant number 1820389]. SEM-EDS data were collected at the University of Southern California Core Center of Excellence in Nano Imaging (CNI). The authors would like to thank Parker Performance Materials for supplying the PTFE membranes used in section 3.1, and especially Stan Merrell and Sarah Propp for their insight and discussions. The authors would also like to thank Dr. Syeed Md Iskander and Dr. Adam Smith for supplying the electrospun membranes used in section 3.3

Appendix A. Supplementary data

Supplementary data to this article can be found online at https://doi.org/10.1016/j.memsci.2021.119947.

References

- F. Suárez, J.A. Ruskowitz, S.W. Tyler, A.E. Childress, Renewable water: direct contact membrane distillation coupled with solar ponds, Appl. Energy 158 (2015) 532–539.
- [2] F. Suárez, S.W. Tyler, A.E. Childress, A theoretical study of a direct contact membrane distillation system coupled to a salt-gradient solar pond for terminal lakes reclamation, Water Res. 44 (2010) 4601–4615.
- [3] R.D. Gustafson, S.R. Hiibel, A.E. Childress, Membrane distillation driven by intermittent and variable-temperature waste heat: system arrangements for water production and heat storage, Desalination 448 (2018) 49–59.
- [4] G. Rao, S.R. Hiibel, A. Achilli, A.E. Childress, Factors contributing to flux improvement in vacuum-enhanced direct contact membrane distillation, Desalination 367 (2015) 197–205.
- [5] C.R. Martinetti, A.E. Childress, T.Y. Cath, High recovery of concentrated RO brines using forward osmosis and membrane distillation, J. Membr. Sci. 331 (2009) 21, 20
- [6] A. Deshmukh, C. Boo, V. Karanikola, S. Lin, A.P. Straub, T. Tong, D.M. Warsinger, M. Elimelech, Membrane distillation at the water-energy nexus: limits, opportunities, and challenges, Energy Environ. Sci. 11 (2018) 1177–1196.
- [7] T. Horseman, Y. Yin, K.S. Christie, Z. Wang, T. Tong, S. Lin, Wetting, scaling, and fouling in membrane distillation: state-of-the-art insights on fundamental mechanisms and mitigation strategies, ACS ES&T Eng. (2020).
- [8] T.Y. Cath, D. Adams, A.E. Childress, Membrane contactor processes for wastewater reclamation in space: II. Combined direct osmosis, osmotic distillation, and membrane distillation for treatment of metabolic wastewater, J. Membr. Sci. 257 (2005) 111–119.
- [9] T.Y. Cath, V.D. Adams, A.E. Childress, Experimental study of desalination using direct contact membrane distillation: a new approach to flux enhancement, J. Membr. Sci. 228 (2004) 5–16.
- [10] G. Rao, S.R. Hiibel, A.E. Childress, Simplified flux prediction in direct-contact membrane distillation using a membrane structural parameter, Desalination 351 (2014) 151–162.

- [11] H. Chang, B. Liu, Z. Zhang, R. Pawar, Z. Yan, J.C. Crittenden, R.D. Vidic, A critical review of membrane wettability in membrane distillation from the perspective of interfacial interactions, Environ. Sci. Technol. (2020).
- [12] M. Rezaei, D.M. Warsinger, J.H. Lienhard V, M.C. Duke, T. Matsuura, W. M. Samhaber, Wetting phenomena in membrane distillation: mechanisms, reversal, and prevention, Water Res. 139 (2018) 329–352.
- [13] L.M. Camacho, L. Dumée, J. Zhang, J.-d. Li, M. Duke, J. Gomez, S. Gray, Advances in membrane distillation for water desalination and purification applications, Water 5 (2013) 94–196.
- [14] E. Drioli, A. Ali, F. Macedonio, Membrane distillation: recent developments and perspectives, Desalination 356 (2015) 56–84.
- [15] R.D. Gustafson, A.L. McGaughey, W. Ding, S.C. McVety, A.E. Childress, Morphological changes and creep recovery behavior of expanded polytetrafluoroethylene (ePTFE) membranes used for membrane distillation, J. Membr. Sci. 584 (2019) 236–245.
- [16] E.W. Washburn, The dynamics of capillary flow, Phys. Rev. 17 (1921) 273.
- [17] B.-S. Kim, P. Harriott, Critical entry pressure for liquids in hydrophobic membranes, J. Colloid Interface Sci. 115 (1987) 1–8.
- [18] E. Guillen-Burrieza, A. Servi, B.S. Lalia, H.A. Arafat, Membrane structure and surface morphology impact on the wetting of MD membranes, J. Membr. Sci. 483 (2015) 94–103.
- [19] H. Chamani, P. Yazgan-Birgi, T. Matsuura, D. Rana, M.I.H. Ali, H.A. Arafat, C. Q. Lan, CFD-based genetic programming model for liquid entry pressure estimation of hydrophobic membranes, Desalination 476 (2020), 114231.
- [20] A.T. Servi, J. Kharraz, D. Klee, K. Notarangelo, B. Eyob, E. Guillen-Burrieza, A. Liu, H.A. Arafat, K.K. Gleason, A systematic study of the impact of hydrophobicity on the wetting of MD membranes, J. Membr. Sci. 520 (2016) 850–859.
- [21] G. Rácz, S. Kerker, Z. Kovács, G. Vatai, M. Ebrahimi, P. Zermak, Theoretical and experimental approaches of liquid entry pressure determination in membrane distillation processes, Period. Polytech. - Chem. Eng. 58 (2014) 81–91.
- [22] P. Jacob, S. Laborie, C. Cabassud, Visualizing and evaluating wetting in membrane distillation: new methodology and indicators based on Detection of Dissolved Tracer Intrusion (DDTI), Desalination 443 (2018) 307–322.
- [23] A. McGaughey, R. Gustafson, A. Childress, Effect of long-term operation on membrane surface characteristics and performance in membrane distillation, J. Membr. Sci. 543 (2017) 143–150.
- [24] F. Villa, M. Marengo, J. De Coninck, A new model to predict the influence of surface temperature on contact angle, Sci. Rep. 8 (2018) 1–10.
- [25] K.G. Nayar, D. Panchanathan, G.H. McKinley, J.H. Lienhard, Surface tension of seawater, J. Phys. Chem. Ref. Data 43 (2014), 043103.
- [26] P. Leroy, A. Lassin, M. Azaroual, L. André, Predicting the surface tension of aqueous 1:1 electrolyte solutions at high salinity, Geochem. Cosmochim. Acta 74 (2010) 5427–5442.
- [27] M.E. Haagh, N. Schilderink, M.H. Duits, I. Siretanu, F. Mugele, I.R. Collins, Salinity-dependent contact angle alteration in oil/brine/silicate systems: the effect of temperature, J. Petrol. Sci. Eng. 165 (2018) 1040–1048.
- [28] P. Yazgan-Birgi, M.I.H. Ali, H.A. Arafat, Estimation of liquid entry pressure in hydrophobic membranes using CFD tools, J. Membr. Sci. 552 (2018) 68–76.
- [29] A.L. McGaughey, P. Karandikar, M. Gupta, A.E. Childress, Hydrophobicity versus pore size: polymer coatings to improve membrane wetting resistance for membrane distillation, ACS Appl. Polym. Mater. 2 (2020) 1256–1267.
- [30] K.W. Lawson, D.R. Lloyd, Membrane distillation. I. Module design and performance evaluation using vacuum membrane distillation, J. Membr. Sci. 120 (1996) 111–121.
- [31] K.S. Christie, T. Horseman, S. Lin, Energy efficiency of membrane distillation: simplified analysis, heat recovery, and the use of waste-heat, Environ. Int. 138 (2020), 105588.
- [32] M. Mulder, J. Mulder, Basic Principles of Membrane Technology, Springer Science & Business Media, 1996.
- [33] C. Li, X. Li, X. Du, Y. Zhang, W. Wang, T. Tong, A.K. Kota, J. Lee, Elucidating the trade-off between membrane wetting resistance and water vapor flux in membrane distillation, Environ. Sci. Technol. 54 (2020) 10333–10341.
- [34] M.R. Qtaishat, T. Matsuura, 13 Modelling of pore wetting in membrane distillation compared with pervaporation, in: Pervaporation, Vapour Permeation and Membrane Distillation, Woodhead Publishing, Oxford, 2015, pp. 385–413.
- [35] M. Gryta, M. Barancewicz, Influence of morphology of PVDF capillary membranes on the performance of direct contact membrane distillation, J. Membr. Sci. 358 (2010) 158–167.
- [36] M. Gryta, Influence of polypropylene membrane surface porosity on the performance of membrane distillation process, J. Membr. Sci. 287 (2007) 67–78.
- [37] W. Wang, X. Du, H. Vahabi, S. Zhao, Y. Yin, A.K. Kota, T. Tong, Trade-off in membrane distillation with monolithic omniphobic membranes, Nat. Commun. 10 (2019) 1–9.
- [38] P. Jacob, B. Dejean, S. Laborie, C. Cabassud, An optical in-situ tool for visualizing and understanding wetting dynamics in membrane distillation, J. Membr. Sci. 595 (2020), 117587.

- [39] E. Guillen-Burrieza, M. Mavukkandy, M. Bilad, H. Arafat, Understanding wetting phenomena in membrane distillation and how operational parameters can affect it, J. Membr. Sci. 515 (2016) 163–174.
- [40] C.F. Couto, M.C.S. Amaral, L.C. Lange, L.V. de Souza Santos, Effect of humic acid concentration on pharmaceutically active compounds (PhACs) rejection by direct contact membrane distillation (DCMD), Separ. Purif. Technol. 212 (2019) 020, 028
- [41] K.A. Salls, D. Won, E.P. Kolodziej, A.E. Childress, S.R. Hiibel, Evaluation of semivolatile contaminant transport in a novel, gas-tight direct contact membrane distillation system, Desalination 427 (2018) 35–41.
- [42] H. Attia, S. Alexander, C.J. Wright, N. Hilal, Superhydrophobic electrospun membrane for heavy metals removal by air gap membrane distillation (AGMD), Desalination 420 (2017) 318–329.
- [43] B.J. Deka, E.-J. Lee, J. Guo, J. Kharraz, A.K. An, Electrospun nanofiber membranes incorporating PDMS-aerogel superhydrophobic coating with enhanced flux and improved anti-wettability in membrane distillation, Environ. Sci. Technol. (2019).
- [44] Z. Wang, Y. Chen, X. Sun, R. Duddu, S. Lin, Mechanism of pore wetting in membrane distillation with alcohol vs. surfactant, J. Membr. Sci. 559 (2018) 183–195.
- [45] M. Rezaei, D.M. Warsinger, J.H. Lienhard V, W.M. Samhaber, Wetting prevention in membrane distillation through superhydrophobicity and recharging an air layer on the membrane surface, J. Membr. Sci. 530 (2017) 42–52.
- [46] F. Guo, A. Servi, A. Liu, K.K. Gleason, G.C. Rutledge, Desalination by membrane distillation using electrospun polyamide fiber membranes with surface fluorination by chemical vapor deposition, ACS Appl. Mater. Interfaces 7 (2015) 8225–8232.
- [47] C. Boo, J. Lee, M. Elimelech, Engineering surface energy and nanostructure of microporous films for expanded membrane distillation applications, Environ. Sci. Technol. 50 (2016) 8112–8119.
- [48] Z. Wang, Y. Chen, S. Lin, Kinetic model for surfactant-induced pore wetting in membrane distillation, J. Membr. Sci. 564 (2018) 275–288.
- [49] K. Rajwade, A.C. Barrios, S. Garcia-Segura, F. Perreault, Pore wetting in membrane distillation treatment of municipal wastewater desalination brine and its mitigation by foam fractionation, Chemosphere 257 (2020), 127214.
- [50] O. Alrehaili, F. Perreault, S. Sinha, P. Westerhoff, Increasing net water recovery of reverse osmosis with membrane distillation using natural thermal differentials between brine and co-located water sources: impacts at large reclamation facilities, Water Res. 184 (2020), 116134.
- [51] Y. Chen, Z. Wang, G.K. Jennings, S. Lin, Probing pore wetting in membrane distillation using impedance: early detection and mechanism of surfactant-induced wetting, Environ. Sci. Technol. Lett. 4 (2017) 505–510.
- [52] F.E. Ahmed, B.S. Lalia, R. Hashaikeh, Membrane-based detection of wetting phenomenon in direct contact membrane distillation, J. Membr. Sci. 535 (2017) 89–93
- [53] J.H. Börner, V. Herdegen, J.-U. Repke, K. Spitzer, The electrical conductivity of CO2-bearing pore waters at elevated pressure and temperature: a laboratory study and its implications in CO2 storage monitoring and leakage detection, Geophys. J. Int. 203 (2015) 1072–1084.
- [54] R.D. Gustafson, J.R. Murphy, A. Achilli, A stepwise model of direct contact membrane distillation for application to large-scale systems: experimental results and model predictions, Desalination 378 (2016) 14–27.
- [55] Y. Yun, R. Ma, W. Zhang, A.G. Fane, J. Li, Direct contact membrane distillation mechanism for high concentration NaCl solutions, Desalination 188 (2006) 251–262.
- [56] J.A. Bush, J. Vanneste, T.Y. Cath, Membrane distillation for concentration of hypersaline brines from the Great Salt Lake: effects of scaling and fouling on performance, efficiency, and salt rejection, Separ. Purif. Technol. 170 (2016) 78–91.
- [57] C.P. Morrow, N.M. Furtaw, J.R. Murphy, A. Achilli, E.A. Marchand, S.R. Hiibel, A. E. Childress, Integrating an aerobic/anoxic osmotic membrane bioreactor with membrane distillation for potable reuse, Desalination 432 (2018) 46–54.
- [58] L.D. Tijing, Y.C. Woo, M.A.H. Johir, J.-S. Choi, H.K. Shon, A novel dual-layer bicomponent electrospun nanofibrous membrane for desalination by direct contact membrane distillation, Chem. Eng. J. 256 (2014) 155–159.
- [59] S. Lin, S. Nejati, C. Boo, Y. Hu, C.O. Osuji, M. Elimelech, Omniphobic membrane for robust membrane distillation, Environ. Sci. Technol. Lett. 1 (2014) 443–447.
- [60] D.M. Warsinger, A. Servi, G.B. Connors, M.O. Mavukkandy, H.A. Arafat, K. K. Gleason, J.H. Lienhard, Reversing membrane wetting in membrane distillation: comparing dryout to backwashing with pressurized air, Environ. Sci. Water Res. Technol. 3 (2017) 930–939.
- [61] M. Gryta, Long-term performance of membrane distillation process, J. Membr. Sci. 265 (2005) 153–159.
- [62] M. Gryta, Fouling in direct contact membrane distillation process, J. Membr. Sci. 325 (2008) 383–394.
- [63] C.-C. Ho, A.L. Zydney, Measurement of membrane pore interconnectivity, J. Membr. Sci. 170 (2000) 101–112.
- [64] L.D. Tijing, J.-S. Choi, S. Lee, S.-H. Kim, H.K. Shon, Recent progress of membrane distillation using electrospun nanofibrous membrane, J. Membr. Sci. 453 (2014) 435–462.